CHEMISTRY
AN ASIAN JOURNAL
ACES
FULL PAPER

DOI: 10.1002/asia.201300524

A Photoelectrochemical Investigation on the Synergetic Effect between CdS and Reduced Graphene Oxide for Solar-Energy Conversion

Guancai Xie,[a, b] Kai Zhang,[b] Hui Fang,[b, c] Beidou Guo,[b] Ruzhi Wang,*[c] Hui Yan,[c] Liang Fang,*[a] and Jian Ru Gong*[b]

Abstract: CdS modified with reduced graphene oxide (RGO) has been widely demonstrated to be effective in the field of solar-energy conversion. However, the inherent mechanism of this superior property is still not thoroughly understood. Thus the photoelectrochemical method was employed to systemically investigate the synergetic effect between CdS and RGO. The result shows that the photoelectrochemical properties of RGO/CdS samples are sensitive to the relative ratio of RGO to CdS, and the photoelectrode with 1.0 wt% ratio of RGO possesses the best photoelectrochemical performance. Further investigation demonstrates that the synergetic effect between CdS and RGO directly influences the charge-transport property and band-structure of the composite, which is also supported by the X-ray photoelectron spectroscopy data and first-principle simulation, respectively.

Keywords: electrochemistry · electronic structure · graphene · photochemistry · semiconductors

Introduction

Progressive initiatives for efficient harvest and conversion of solar energy are urgently needed to meet our demand for renewable and clean energy.[1] However, the lack of effective functional materials has severely restricted further development in this vital field. As is known, CdS is an important material for solar-energy conversion because of its narrow bandgap (≈2.4 eV), and relatively high conduction-band position (−0.7 V versus the normal hydrogen electrode (NHE); pH 0). Unfortunately, CdS nanoparticles always suffer from rapid electron–hole recombination, which heavily retards their photoconversion efficiency.[2] Recently, graphene as a building block for novel functional nanomaterials has attracted much attention for applications in solar-energy conversion such as photocatalysis,[3] solar cells,[4] and solar fuels[5] due to its novel two-dimensional honeycomb crystal structure and superior electronic properties.[6] Many works demonstrate that nanomaterials modified with graphene always show remarkable enhancement of the photoconversion efficiency relative to the bare nanomaterials because graphene can act as an excellent electron reservoir to separate and transfer photoinduced carriers effectively.[3,7] Hence, intensive scientific works have been focused on the enhancement of the photocatalytic or photovoltaic performance of CdS by introducing graphene.[8] For example, our group[8a] has demonstrated that CdS/graphene nanocomposite exhibited enhanced photocatalytic H_2-production activity relative to CdS nanoparticles. Xu et al.[8c] have reported that N-graphene as a charge collector can promote separation and transfer of the photogenerated carriers in CdS.

The photoconversion efficiency of the CdS/graphene nanomaterial generally varies with the ratio of graphene in the nanocomposite, and tuning the relative ratio of graphene to CdS is an effective strategy to achieve the optimal photoconversion efficiency. The improved photoconversion efficiency is mainly attributed to the unique abilities of graphene to efficiently separate the photoinduced carriers and consequently hinder the recombination of electrons and holes in CdS nanoparticles. Recently, some theoretical research[9] has shown that, in addition to the promotion of the separation of photogenerated charges, the interaction between semiconductor nanoparticle and graphene can also modify the band structure of the nanocomposite, thus leading to the extended light absorption of the nanocomposite. Unfortunately, the interaction between CdS and graphene is given less consideration in previous reports. Consequently, a systematic investigation of the synergetic interaction be-

[a] G. Xie,[+] Prof. L. Fang
Department of Applied Physics
Chongqing University
Chongqing 400044 (P. R. China)
Fax: 86-23-65678369
E-mail: fangliangcqu@yahoo.com.cn

[b] G. Xie,[+] Dr. K. Zhang,[+] Dr. H. Fang, B. Guo, Prof. J. R. Gong
National Center for Nanoscience and Technology
11 Zhongguancun Beiyitiao
Beijing 100190 (P. R. China)
Fax: 86-10-62656765
E-mail: gongjr@nanoctr.cn

[c] Dr. H. Fang, Prof. R. Wang, Prof. H. Yan
Laboratory of Thin Film Materials
College of Materials Science and Engineering
Beijing University of Technology
Beijing 100124 (P.R. China)
Fax: 86-10-67392445
E-mail: wrz@bjut.edu.cn

[+] These authors contributed equally to this work.

Supporting information for this article is available on the WWW under http://dx.doi.org/10.1002/asia.201300524.

tween CdS and graphene is highly desired for an in-depth understanding of the enhancement of the photoconversion efficiency.

In recent years, electrochemical methods, particularly cyclic voltammetry (CV) and electrochemical impedance spectra (EIS), have been widely used to analyze the electronic properties of semiconductor materials.[10] CV has been successfully employed for several decades in the quantitative estimation of the highest occupied molecular orbital (HOMO) and lowest unoccupied molecular orbital (LUMO) levels of polymers[11] and semiconductors[12] because of the mild experimental conditions relative to other methods such as photoelectron spectroscopy. Meanwhile, EIS can reveal the valuable information about the charge-transfer kinetics of a photoelectrochemical cell, and the frequency response shown by EIS can help identify the charge-transfer resistance at an electrode interface.

Herein, CdS/RGO electrodes with different reduced graphene oxide (RGO) contents were prepared and systemically investigated by photoelectrochemical methods combined with first-principle simulation to gain an in-depth understanding of the origin of the excellent solar-energy conversion efficiency of the CdS/RGO composite. Both the change in charge-separation ability and the influence on band structure of these CdS/RGO nanomaterials are discussed in detail.

Results and Discussion

CdS/RGO samples with several typical RGO contents, that is, 0.5, 1.0, and 5.0 wt%, were prepared by a solvothermal method and fabricated into thin film eletrodes by the doctor-blade method followed by calcination. The obtained products were labeled as GC0.5, GC1.0, and GC5.0, respectively. Pure CdS (GC0) was also prepared by using the same method in the absence of graphene oxide (GO). The phases of the calcined GCx ($x=0$, 0.5, 1.0, and 5.0) samples were first determined by X-ray diffraction (XRD) measurement, as depicted in Figure 1. For the calcined GC0, all of the diffraction peaks can be satisfactorily indexed as the hexagonal CdS phase (JCPDS 41-1049), which is different from the uncalcined GC0 sample with the cubic phase.[8a] The phase transition from cubic to hexagonal CdS is caused by the high-temperature calcination process.[13] After the introduction of RGO, a mixture of cubic (JCPDS 10-0454) and hexagonal CdS phases could be observed for GC0.5, GC1.0, and GC5.0 samples in the present study. That is, the addition of RGO can partially suppress the phase-transition process of CdS during the calcination process.

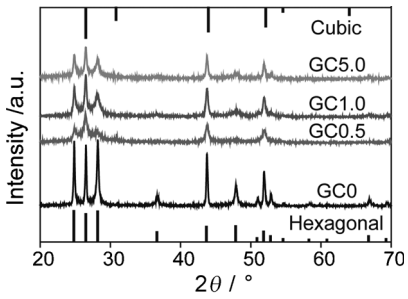

Figure 1. XRD patterns of GC0, GC0.5, GC1.0, and GC5.0 samples after calcination treatment.

Transmission electron microscopy (TEM) images of the obtained samples are shown in Figure 2. It is clear that pure CdS aggregates to form larger particles with diameters of approximately 300 nm (Figure 2a). Figure 2b–d, however, shows that much smaller CdS nanoparticles are almost uniformly and tightly spread on the RGO sheets for GC0.5, GC1.0, and GC5.0 samples. Although the high-temperature process partially induced the phase transition from a cubic to hexagonal structure, there is almost no influence on the dispersion of CdS nanoparticles. This is in accordance with our previous report,[8a] as graphene can efficiently anchor the CdS nanoparticles and inhibit aggregation of CdS nanoparticles in the CdS/RGO composites. Consequently, the partial suppression of phase transition by graphene is reasonable, because the phase change always starts from the interface of the contact particles.[14]

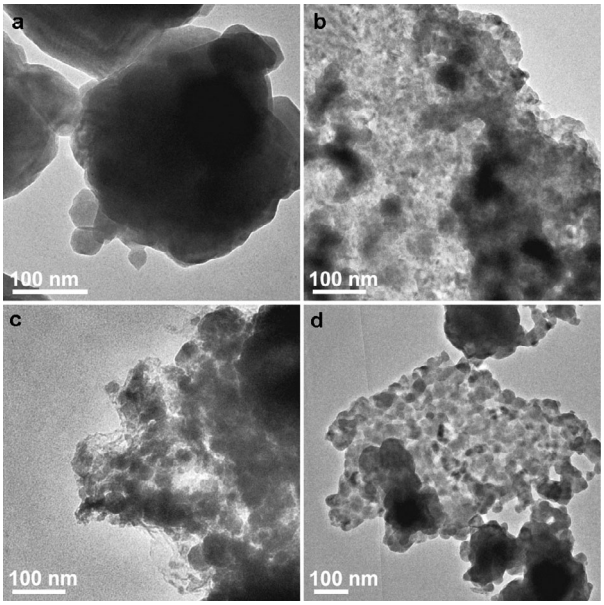

Figure 2. TEM images of a) GC0, b) GC0.5, c) GC1.0, and a) GC5.0 after calcination treatment.

To verify the effect of RGO content on the photoconversion properties of CdS/RGO composites, the photoelectrochemical properties of the samples were investigated. Figure 3 shows a comparison of the photocurrent density/applied potential (J–V) characteristics of the photoelectrochemical (PEC) cells fabricated from the CdS/RGO electrodes under visible light in the potential range from 0 to 0.5 V (versus Ag/AgCl). Compared to pure CdS, an increase in the photocurrent density at 0 V bias can be seen for GC0.5 in Figure 3, and the photocurrent density of the GC1.0

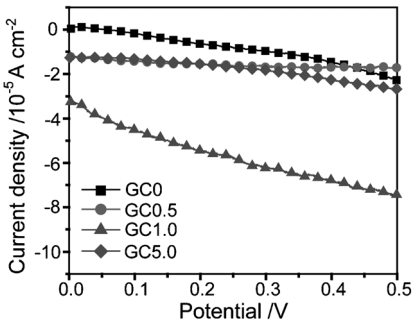

Figure 3. Photocurrent density-applied potential plots for the cells with GC0, GC0.5, GC1.0, and GC5.0 electrodes.

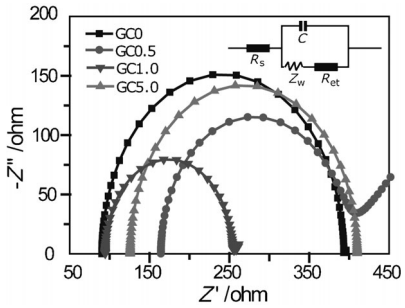

Figure 5. Nyquist impedance plots of GC0, GC0.5, GC1.0, and GC5.0 electrodes in 0.1 M KNO_3 aqueous solution under visible-light irradiation.

sample achieves the maximum value. With further increasing the RGO content to 5 wt% ratio, the cell performance begins to decrease. The as-prepared electrodes exhibit a similar energy conversion tendency with increasing graphene content with respect to photocatalytic hydrogen production.[8a]

The transient photocurrent responses of GC0, GC0.5, GC1.0, and GC5.0 photoelectrodes were recorded for typical on/off cycles of intermittent visible-light irradiation (≈60 s) at a bias potential of 0.5 V, as shown in Figure 4, to

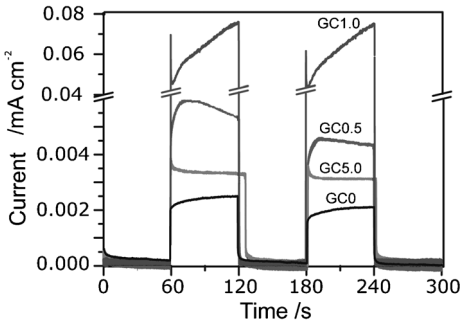

Figure 4. The transient photocurrent responses of GC0, GC0.5, GC1.0, and GC5.0 electrodes.

further prove the enhancement of the photoelectrochemical performance. It can be seen that the photocurrent density is drastically increased when the irradiation is on, and the GC1.0 sample shows the highest photocurrent density relative to other samples, which is in accordance with the *J*–*V* observation. Also, the appearance of an anodic photocurrent spike at the initial irradiation can be derived from the separation of photoinduced electron–hole pairs.[15] Moreover, a significant photocurrent decay is observed in the transient photocurrent responses of GC0 and GC0.5 samples, whereas no obvious photocurrent decay is observed for the GC1.0 photoelectrode. The result suggests that the photogenerated carriers can be separated effectively in the GC1.0 sample.[10b]

The charge-transfer property of the photoelectrode also plays an important role in determining the photoelectrochemical performance. Thus, EIS of the as-prepared electrodes was measured, as shown in Figure 5. The Nyquist plots of the four electrodes were fitted by using the typical Randles circuit,[16] in which R_s, R_{et}, Z_w, and C represent the resistance of the electrolyte solution, electron-transfer resistance, Warburg impedance, and electrode/electrolyte interface capacitance, respectively, as illustrated in the inset of Figure 5. Herein, the high-frequency arc corresponds to the charge-transfer resistance (R_{et}) at the contact interface between the electrode and the electrolyte solution, and the fitted R_{et} of GC0, GC0.5, GC1.0, and GC5.0 are 302.7, 225.9, 159.2, and 284.3 Ω cm^2, respectively. Apparently, the charge-transfer resistance of the GC1.0 electrode is much smaller than those of other electrodes, thus indicating its excellent charge-transfer property, which is also agreement with the above photocurrent response.

To thoroughly reveal the origin of this high charge-transfer property, X-ray photoelectron spectroscopy (XPS) analyses were performed to confirm the reduction level of RGO in the samples. As shown in Figure 6, three peaks are observed in the C 1s deconvolution spectra of GC0.5, GC1.0, and GC2.0 samples, which correspond to sp^2-bonded carbon (C–C, 284.8 eV), epoxy/hydroxyl groups (C–O, 286.9 eV),

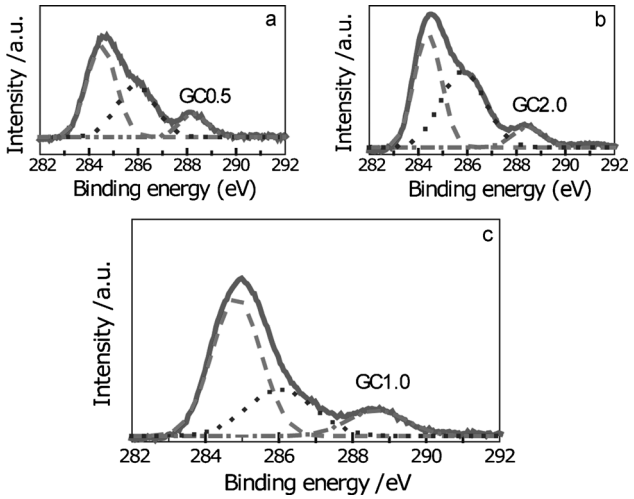

Figure 6. High-resolution XPS spectra of C 1s from GC0.5, GC1.0, and GC2.0 samples, which can be deconvoluted into three Lorentzian peaks at 284.8, 286.9, and 288.9 eV.

and carboxyl (O−C=O, 288.9 eV), respectively. The lower intensities of C−O and O−C=O peaks indicate the further removal of the oxygen-containing functional groups for GC1.0. The amount of oxygen-containing groups can also be monitored by the relative content of graphitic carbon by the following equation [Eq. (1)]:

$$\text{graphitic carbon\%} = \frac{A_{C-C}}{A_{C-C} + A_{C-O} + A_{O-C=C}} \times 100\% \qquad (1)$$

in which A_{C-C}, A_{C-O}, and $A_{O-C=O}$ are the peak areas for C−C, C−O, and O−C=O, respectively. GC1.0 was found to have the highest graphitic carbon of 59%, whereas the graphitic carbon for GC0.5 and GC2.0 samples decreases to 41 and 44%, respectively. As known, RGO undergoes an insulator–semiconductor–semimetal transition with the increase of its reduction degree.[17] And, RGO with higher reduction degree possesses higher electronic conductivity, thereby resulting in a better transfer property. Thus, GC1.0 should possess higher electronic conductivity than other samples, and the best performance of GC1.0 is reasonable because of its ability for efficient separation and transfer of the photogenerated carriers, which is also in accordance with the transient photocurrent response and EIS as discussed before.

However, as mentioned above, it is not appropriate to attribute the improved photoelectrochemical performance solely to the enhanced charge-separation and -transfer ability. It has been reported that graphene can be used to modulate the bandgap of semiconductors.[18] For example, in graphene–TiO_2 photocatalysts, the bandgap of the nanocomposites was found to decrease along with the increase in graphene content because of the interfacial electron coupling between graphene and TiO_2.[18a] Thus, to gain an in-depth understanding on the other origin of the excellent property, we will investigate the influence of RGO on the band structure of the nanocomposite, and more thoroughly reveal the inherent mechanism of the high charge-separation ability.

CV was performed on these photoelectrodes to probe the effect of the synergetic effect on the band-structure variation. According to the reported equations,[19] the HOMO and LUMO levels [eV] of the samples can be evaluated by Equations (2) and (3):

$$E_{LUMO} = -(E_{red} + 4.4)\ \text{eV} \qquad (2)$$

$$E_{HOMO} = -(E_{ox} + 4.4)\ \text{eV} \qquad (3)$$

in which E_{red} and E_{ox} are the onset of reduction and oxidation potential, respectively. The electrochemical bandgap can then be derived from the difference between the reduction potential and the oxidation potential. As shown in Figure 7, the HOMO and LUMO level of the GC0 sample were calculated to be −6.14 and −3.28 eV, respectively, which are close to the reported energy levels of CdS nanoparticles.[20] The variation in the onset potential indicates that the LUMO achieves the highest level at an RGO content of 0.5%. Following a further increase in the ratio, the LUMO level decreases and tends to be stable. First-principle calculations on the density functional theory (DFT) were also performed with the VASP code[21] for further understanding of the shifting of the LUMO and HOMO levels (see the Supporting Information). The result shows that the work function of CdS is 5.24 and 5.27 eV for the hexagonal and cubic phase, respectively. After the introduction of graphene, the work function of the graphene-hexagonal CdS and graphene-cubic CdS system decreases to 3.82 and 4.30 eV, respectively, which is in agreement with the decrease in the electrochemical LUMO levels. The larger decrease in the LUMO level from the theoretical result relative to that of the experimental results might be attributed to the quantum-confinement effect by the CdS quantum dot that is not present in experimental systems. Normally, a higher LUMO energy level possesses an increased driving force for the injection of electrons to the H^+/H_2 reduction level, thereby benefitting the photoelectrochemical performance.[22] This significant role of graphene further demonstrates that the synergetic interaction between RGO and CdS affects the band structure of the CdS/RGO composite. Meanwhile, the electrochemical bandgap of the samples is 2.86 eV for the GC0 sample, and it decreases with the increase in the RGO content of the CdS/RGO samples, which is in agreement with the variation in the optical bandgap (see the Supporting Information). The larger electrochemical bandgap relative to the optical bandgap is attributed to the extra energy requirement beyond the bandgap for redox in the electrochemical system.[12b] Generally, the bandgap narrowing is favorable for light absorption, which could be a reason for the enhancement of the photoelectrochemical performance for the CdS/RGO electrodes. Therefore, we believe that the optimum bandgap and the moderate LUMO level should also be responsible for the optimal performance of the GC1.0 samples, which is also supported by the phenomena of the balance between the bandgap and the conduction-band position in the $Cd_{1-x}Zn_xS$ solid-solution photocatalyst system.[23]

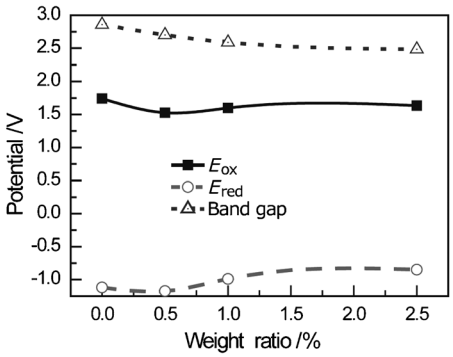

Figure 7. The onset reduction (E_{red}) and oxidation (E_{ox}) potentials versus the Ag/AgCl reference electrode. The difference between E_{ox} and E_{red} can be used to estimate the electrochemical bandgap. The horizontal axis is the weight ratios of RGO.

Conclusion

In summary, the photoelectrochemical properties of various CdS/RGO photoelectrodes that had different weight ratios of RGO were investigated. The EIS and XPS spectra demonstrated that the different charge-separation and -transfer properties of CdS/RGO samples were in close relationship with the reduction level of RGO in the composites. The observation of electrochemical CV combined with the first-principle simulation indicated the successful modulation of the band structure by varying the RGO content. Owing to the synergetic effect between CdS and RGO on the band-structure and charge-transfer property, CdS/RGO samples exhibited improved photoelectrochemical performances relative to pure CdS, and the GC1.0 sample possessed the best photoelectrochemical performance, which should be ascribed to maximizing the synergetic effect. This study provides a new insight into the inherent mechanism of the excellent photoelectrochemical performance of the graphene-based composite, and will shed light on the future works of solar-energy conversion applications of graphene-based materials.

Experimental Section

Synthesis of CdS/RGO Nanocomposites

GO powders were prepared from graphite powder according to a modified Hummers' method.[24] The as-prepared GO and $Cd(Ac)_2{\cdot}2H_2O$ (2 mmol, ≈98.5%, Aladdin) were dispersed in dimethyl sulfoxide (DMSO; 80 mL). The weight ratio of GO to $Cd(Ac)_2{\cdot}2H_2O$ was 0, 0.5, 1.0, 2.0, 2.5, and 5%. After vigorous stirring and sonication, the solution was transferred into a Teflon-lined autoclave (80 mL) and left at 180°C for 12 h. The obtained solution was cooled to room temperature naturally. Next, the leaching bottle with a microporous membrane filter (0.22 μm) was used to obtain the precipitate and remove the residue of DMSO with acetone, alcohol, and deionized (DI) water. The final product was dried in an oven at 60°C for 12 h, and the seven obtained samples were labeled GC0, GC0.5, GC1.0, GC2.0, GC2.5, and GC5.0, respectively.

Characterization of the Materials

Crystallographic information of the obtained samples were determined by X-ray diffraction with a D/MAX-2500 diffractometer (Rigaku, Japan) with $Cu_{K\alpha}$ radiation source ($\lambda = 1.54056$ Å). Transmission electron microscopy images were collected with a Tecnai G2 20 S-TWIN electron microscope. X-ray photoelectron spectroscopy data were obtained with an ESCALab 220i-XL electron spectrometer from VG Scientific using 300 W $Al_{K\alpha}$ radiation. All binding energies were referenced to the C1s peak (284.8 eV) that arises from surface hydrocarbons.

Photoelectrochemical Experiments

To prepare the CdS/RGO electrode, the CdS/RGO samples (5 mg) were mixed with ethanol (417 μL) that contained acetylacetone (41.7 μL) and Triton X-100 (41.7 μL) to form a homogeneous colloid. Then the colloid was coated onto conducting indium–tin oxide (ITO) glass by using the doctor-blade technique. After air drying, the electrode was calcined for 30 min at 450°C under a nitrogen atmosphere. Photoelectrochemical measurements were performed with a homemade three-electrode system connected to a CHI-660B workstation (Shanghai Chenhua Limited, China). The modified ITO electrode was used as the working electrode, Pt wire as the counter electrode, Ag/AgCl as the reference electrode, and 0.1 M KNO_3 as the electrolyte. A 350 W Xe lamp with cutoff filters ($\lambda > 420$ nm) was used as a source of visible light.

Acknowledgements

The authors acknowledge partial financial support for this work from the National Natural Science Foundation of China (grant nos. 91123003, 21005023), the National Basic Research Program of China (grant no. 2011CB933401), and the Knowledge Innovation Program of the Chinese Academy of Sciences.

[1] a) C. M. Elliott, *Nat. Chem.* **2011**, *3*, 188–189; b) A. Paracchino, V. Laporte, K. Sivula, M. Grätzel, E. Thimsen, *Nat. Mater.* **2011**, *10*, 456–461; c) K. Zhang, Q. Liu, H. Wang, R. Zhang, C. Wu, J. R. Gong, *Small* **2013**, DOI: 10.1002/smll.201300841; d) Q. Li, H. Meng, P. Zhou, Y. Zheng, J. Wang, J. Yu, J. R. Gong, *ACS Catal.* **2013**, *3*, 882–889; e) C. Li, J. Wang, B. Wang, J. R. Gong, Z. Lin, *Mater. Res. Bull.* **2012**, *47*, 333–337; f) C. Li, G. Xu, B. Zhang, J. R. Gong, *Appl. Catal. B* **2012**, *115–116*, 201–208; g) C. Li, J. Wang, B. Wang, J. R. Gong, Z. Lin, *J. Nanosci. Nanotechnol.* **2012**, *12*, 2496–2502; h) J. Zhang, J. Yu, Y. Zhang, Q. Li, J. R. Gong, *Nano Lett.* **2011**, *11*, 4774–4779.

[2] a) K. Zhang, L. J. Guo, *Catal. Sci. Technol.* **2013**, *3*, 1672–1690; b) N. Zhang, Y. H. Zhang, X. Y. Pan, X. Z. Fu, S. Q. Liu, Y. J. Xu, *J. Phys. Chem. C* **2011**, *115*, 23501–23511.

[3] a) Q. Xiang, J. Yu, M. Jaroniec, *Chem. Soc. Rev.* **2012**, *41*, 782–796; b) W. S. Wang, D. H. Wang, W. G. Qu, L. Q. Lu, A. W. Xu, *J. Phys. Chem. C* **2012**, *116*, 19893–19901; c) D. H. Wang, L. Jia, X. L. Wu, L. Q. Lu, A. W. Xu, *Nanoscale* **2012**, *4*, 576–584; d) G. Xie, K. Zhang, B. Guo, Q. Liu, L. Fang, J. R. Gong, *Adv. Mater.* **2013**, DOI: 10.1002/adma.201301207.

[4] Y. B. Tang, C. S. Lee, J. Xu, Z. T. Liu, Z. H. Chen, Z. He, Y. L. Cao, G. Yuan, H. Song, L. Chen, L. Luo, H. M. Cheng, W. J. Zhang, I. Bello, S. T. Lee, *ACS Nano* **2010**, *4*, 3482–3488.

[5] Y. T. Liang, B. K. Vijayan, K. A. Gray, M. C. Hersam, *Nano Lett.* **2011**, *11*, 2865–2870.

[6] a) A. K. Geim, K. S. Novoselov, *Nat. Mater.* **2007**, *6*, 183–191; b) B. Guo, L. Fang, B. Zhang, J. R. Gong, *Insciences J.* **2011**, *1*, 80–89; c) B. Guo, Q. Liu, E. Chen, H. Zhu, L. Fang, J. R. Gong, *Nano Lett.* **2010**, *10*, 4975–4980; d) B. Guo, L. Fang, B. Zhang, J. R. Gong, *Electron. Lett.* **2011**, *47*, 663–664; e) Q. Liu, B. Guo, Z. Rao, B. Zhang, J. R. Gong, *Nano Lett.* **2013**, *13*, 2436–2441.

[7] a) N. Yang, J. Zhai, D. Wang, Y. Chen, L. Jiang, *ACS Nano* **2010**, *4*, 887–894; b) H. Zhang, X. Lv, Y. Li, Y. Wang, J. Li, *ACS Nano* **2010**, *4*, 380–386.

[8] a) Q. Li, B. Guo, J. Yu, J. Ran, B. Zhang, H. Yan, J. R. Gong, *J. Am. Chem. Soc.* **2011**, *133*, 10878–10884; b) A. Ye, W. Fan, Q. Zhang, W. Deng, Y. Wang, *Catal. Sci. Technol.* **2012**, *2*, 969–978; c) L. Jia, D. H. Wang, Y. X. Huang, A. W. Xu, H. Q. Yu, *J. Phys. Chem. C* **2011**, *115*, 11466–11473.

[9] a) A. Du, S. Sanvito, Z. Li, D. Wang, Y. Jiao, T. Liao, Q. Sun, Y. H. Ng, Z. Zhu, R. Amal, S. C. Smith, *J. Am. Chem. Soc.* **2012**, *134*, 4393–4397; b) R. Long, N. J. English, O. V. Prezhdo, *J. Am. Chem. Soc.* **2012**, *134*, 14238–14248; c) C. Dong, X. Li, P. Jin, W. Zhao, J. Chu, J. Qi, *J. Phys. Chem. C* **2012**, *116*, 15833–15838; d) A. Du, Y. H. Ng, N. J. Bell, Z. Zhu, R. Amal, S. C. Smith, *J. Phys. Chem. Lett.* **2011**, *2*, 894–899.

[10] a) T. Berger, D. Monllor-Satoca, M. Jankulovska, T. Lana-Villarreal, R. Gómez, *ChemPhysChem* **2012**, *13*, 2824–2875; b) J. Zhang, J. Yu, M. Jaroniec, J. R. Gong, *Nano Lett.* **2012**, *12*, 4584–4589.

[11] J. Hou, H. Y. Chen, S. Zhang, G. Li, Y. Yang, *J. Am. Chem. Soc.* **2008**, *130*, 16144–16145.

[12] a) Y. Li, Y. Hu, Y. Zhao, G. Shi, L. Deng, Y. Hou, L. Qu, *Adv. Mater.* **2011**, *23*, 776–780; b) S. N. Inamdar, P. P. Ingole, S. K. Haram, *ChemPhysChem* **2008**, *9*, 2574–2579.

[13] H. Metin, R. Esen, *J. Cryst. Growth* **2003**, *258*, 141–148.

[14] R. L. Penn, J. F. Banfield, *Am. Mineral.* **1998**, *83*, 1077–1082.
[15] Y. H. Ng, A. Iwase, A. Kudo, R. Amal, *J. Phys. Chem. Lett.* **2010**, *1*, 2607–2612.
[16] J. E. B. Randles, *Discuss. Faraday Soc.* **1947**, *1*, 11–19.
[17] G. Eda, C. Mattevi, H. Yamaguchi, H. Kim, M. Chhowalla, *J. Phys. Chem. C* **2009**, *113*, 15768–15771.
[18] a) J. S. Lee, K. H. You, C. B. Park, *Adv. Mater.* **2012**, *24*, 1084–1088; b) X. Yang, H. Cui, Y. Li, J. Qin, R. Zhang, H. Tang, *ACS Catal.* **2013**, *3*, 363–369.
[19] V. Gupta, N. Chaudhary, R. Srivastava, G. D. Sharma, R. Bhardwaj, S. Chand, *J. Am. Chem. Soc.* **2011**, *133*, 9960–9963.
[20] C. X. Guo, H. B. Yang, Z. M. Sheng, Z. S. Lu, Q. L. Song, C. M. Li, *Angew. Chem.* **2010**, *122*, 3078–3081; *Angew. Chem. Int. Ed.* **2010**, *49*, 3014–3017.
[21] G. Kresse, J. Furthmüller, *Phys. Rev. B* **1996**, *54*, 11169–11186.
[22] a) K. Zhang, D. Jing, C. Xing, L. Guo, *Int. J. Hydrogen Energy* **2007**, *32*, 4685–4691; b) A. S. Goncalves, M. R. Davolos, N. Masaki, S. Yanagida, S. Mori, A. F. Nogueira, *J. Appl. Phys.* **2009**, *106*, 064316.
[23] C. Xing, Y. Zhang, W. Yan, L. Guo, *Int. J. Hydrogen Energy* **2006**, *31*, 2018–2024.
[24] Y. Xu, H. Bai, G. Lu, C. Li, G. Shi, *J. Am. Chem. Soc.* **2008**, *130*, 5856–5857.

Received: April 15, 2013
Revised: June 3, 2013
Published online: August 12, 2013

